OPEN ACCESS

Corrosion Behavior of Structural Materials for Potential Use in Nitrate Salts Based Solar Thermal Power Plants

To cite this article: Kodi L. Summers and Dev Chidambaram 2017 *J. Electrochem. Soc.* **164** H5357

JES Focus Issue on Progress in Molten Salts and Ionic Liquids

Corrosion Behavior of Structural Materials for Potential Use in Nitrate Salts Based Solar Thermal Power Plants

Kodi L. Summers* **and Dev Chidambaram****,z

Materials Science and Engineering, University of Nevada, Reno, Reno, Nevada 89557, USA

Commercial and economic success of concentrated solar power (CSP) plants requires operating at maximum efficiency and capacity which necessitates the use of materials that are reliable at high temperatures. This study investigates the corrosion behavior of structural alloys in molten nitrate salts at three temperatures common to CSP plants. Corrosion behavior was evaluated using gravimetric and inductively-coupled plasma optical emission spectroscopy (ICP-OES) analysis. Surface oxide structure and chemistry was characterized using X-ray diffraction and Raman spectroscopy. Electrochemical behavior of candidate structural alloys Alloy 4130, austenitic stainless steel 316, and super-austenitic Incoloy 800H was evaluated using potentiodynamic polarization characteristics. Gravimetric and ICP-OES analysis indicated that Alloy 4130 exhibited the least corrosion resistance at 500°C compared to SS316 and 800H. However, at 300°C, the three alloys exhibited similar weight gain. Electrochemical evaluation of these candidate materials was observed to correlate well with the corrosion behavior observed from gravimetric and ICP-OES analysis. This study identifies that all three alloys exhibited acceptable corrosion rate in 300°C molten salt, while elevated salt temperatures require the more corrosion resistant alloys, stainless steel 316 and 800H. Characterization of the sample surfaces revealed the presence of spinels at lower temperatures, while Fe_2O_3 was the dominant iron oxide at higher temperatures for each alloy.

Manuscript submitted February 16, 2017; revised manuscript received July 1, 2017. Published August 11, 2017. This was Paper 967 presented at San Diego, California, Meeting of the Society, May 29–June 2, 2016. *This paper is part of the JES Focus Issue on Progress in Molten Salts and Ionic Liquids.*

Like all power plants, maximizing the conversion efficiency of solar energy in a concentrated solar power (CSP) plant is essential to minimizing cost and resources while maximizing energy output. The choice of heat transfer fluid is a fundamental parameter in maximizing efficiency of an energy source. A heat transfer fluid that can also function as an energy storage medium for solar energy while being chemically compatible with the structural components of the plant is an ideal candidate for implementation.

Significant research had been performed from 1982 to 1985 on the use of molten salt as a heat transfer medium in solar power applications. Sandia National Laboratory in New Mexico conducted the Molten Salt Electric Experiment (MSEE) which was the first power tower system to use molten nitrate salt as the primary working fluid to produce electricity. This experiment proved the feasibility of using molten salt as a heat transfer medium in a central receiver design along with a two-tank storage system designed to address intermittency.[1] The MSEE used a molten nitrate salt composition of 40% KNO_3 and 60% $NaNO_3$ by weight which is the composition used for the study presented herein.

Corrosion of structural components is determined by the properties of the heat transfer fluid and corrosion resistance of the components in contact with that heat transfer fluid. Depending on the corrosion resistance of the alloy to a high-temperature, oxidizing environment, the alloy will either form an adherent, compact oxide layer that slows the corrosion rate or form an oxide layer that is loose and prone to delamination. The formation of these layers is dependent on the composition of the alloy and strongly influenced by impurities in the salt mixture. Water is a common impurity in salt mixtures due to their hygroscopic nature, and its presence can result in a significant change in the corrosion behavior of the alloy exposed. Electrochemical analysis by Singh[2] showed that the oxidation rate of iron exposed to wet $NaNO_3$ and KNO_3 was 45 and 11% higher than their respective dry melts. Additionally, the presence of sodium chloride in excess of 0.035 mol/kg led to pitting on mild steels.[3]

Numerous studies have been conducted to evaluate the corrosion resistance of various alloys to molten nitrate salts. Long-term exposure studies were conducted in thermal convection loops operating from 300 to 600°C on Incoloy 800, SS304 and SS316 with metal loss rates of 5–12 microns per year at 600°C.[4–6] Isothermal studies were also performed on stainless steels, Cr-Mo steels, low alloy steels, aluminum-coated steels, nickel, aluminum, and titanium. Incoloy 800, aluminum and the aluminized steels saw negligible corrosion, while Inconel 600 underwent internal oxidation, titanium rapidly formed an adherent surface oxide film, and nickel experienced severe intergranular corrosion.[6–8] Additionally, chemical analysis of the salt following exposure studies revealed that chromium was soluble, and iron and nickel have negligible solubility. The solubility of chromate ions in molten nitrates was found to be significant and kinetically limited to amounts below solubility limits of the melt with no observed concentration above the solubility limit after 5000 hours.[6]

Electrochemical analysis of molten nitrate salts has also been performed to evaluate the properties of the molten mixture and its interaction with metals. Molten nitrate salts undergo thermal decomposition resulting in the formation of nitrites and oxygen.[6,9–11] Due to this variable composition with time, an investigation of the decomposition of nitrate salts was conducted via electrochemical methods to determine potential species present in molten salt mixtures as a result of thermal decomposition and salt-metal interactions. One study found that NO_2^- also decomposes to form oxide ions, nitrogen and oxygen gas at temperatures greater than 600°C.[12] However, a study on the passivation of iron in molten nitrate and nitrite salts indicates that the formation of oxide ions occurs in the presence of iron leading to a proposed mechanism of iron oxidation.[9,13,14]

Due to the relative difficulty of performing electrochemistry in a molten salt and correlating electrochemical results to corrosion processes, the use of electrochemistry to perform accelerated corrosion studies of alloys in molten nitrate salt environments has not been done. Herein, the feasibility of electrochemical evaluation of candidate materials for structural components in CSP plants using molten nitrate salts as a heat transfer medium is investigated. Accurate evaluation of candidate materials without expensive and lengthy exposure tests will provide a faster, more economical method of screening materials

*Electrochemical Society Student Member.
**Electrochemical Society Member.
zE-mail: dcc@unr.edu

Table I. Composition of SS316, Alloy 4130 and Incoloy 800H, wt %.

Element	Alloy 4130	SS316	800H
Carbon	0.3	0.0247	0.07
Chromium	0.818	16.6145	20.42
Copper	0.138	0.43	0.04
Manganese	0.46	1.4975	0.58
Molybdenum	0.154	2.0435	—-
Nitrogen	—	0.0368	0.009
Nickel	0.079	10.04	30.49
Phosphorus	0.01	0.036	0.013
Sulfur	0.002	0.001	0.0001
Silicon	0.16	—-	0.38
Aluminum	0.028	—-	0.44
Titanium	—-	—-	0.55
Cobalt	—-	—-	0.03
Iron	Balance	Balance	Balance

in molten nitrate salts. Gravimetric analysis and characterization of corrosion products and surface oxide films are presented to understand the correlation between electrochemical results and corrosion behavior in molten nitrate salts.

Materials and Methods

Alloy 4130 and stainless steel 316 (SS316) were acquired from McMaster-Carr, and Incoloy 800H was supplied by High Performance Alloys, Inc with certified material compositions as shown in Table I. The alloys had the following surface finish and/or heat-treatment from the distributor: Alloy 4130 was annealed and spheroidized, SS316 had a 2B mill finish, and 800H had a 2D mill finish. A 2D mill finish is a uniform, dull finish whereas a 2B mill finish is a bright, more reflective finish. All studies performed on Alloy 4130, SS316, and Incoloy 800H were in an as-received state in order to better simulate an industrial environment in which these alloys are installed as-received. A set of three 800H samples were polished to a 1 μm finish on one face to observe how the 2D mill finish affects corrosion behavior. The salt composition employed for this work was an off-eutectic 60/40 weight percent mixture of American Chemical Society (ACS) reagent grade sodium nitrate ($NaNO_3$) and potassium nitrate (KNO_3) from Alfa Aesar and Amresco, respectively. The salts were dried separately at 170°C for 24 hours in an open-air oven prior to each experiment. Inconel 625 wire was used as the counter electrode for all electrochemical testing presented herein. A pseudo-reference electrode was used in the form of a platinum wire. Alumina crucibles (GraphiteStore.com, >99.6%) were used to contain the molten salt and samples for the duration of all experiments performed.

Prior to sample exposure, each sample was degreased with acetone, rinsed with deionized water and allowed to air dry before recording pre-exposure weight. Each alloy was exposed to every set of conditions in triplicate. All exposures were performed under a fume hood in atmospheric conditions. Samples were exposed to 300, 400 and 500°C molten nitrate salt for 100 hours with an additional exposure for 350 hours at 500°C. Upon completion of the exposure, the samples were removed from the molten salt mixture and placed in a desiccant container to cool to room temperature. The samples were then removed from the desiccant container and rinsed with deionized water to remove any residual salt. The samples were then rinsed with isopropanol before drying in a desiccant container overnight prior to being weighed. Weight gain rates for triplicate samples exposed to the same salt were averaged.

Electrochemical testing was performed using a standard three-electrode configuration. A platinum wire pseudo-reference and Inconel 625 counter electrode were utilized for all electrochemical tests. Potentiodynamic polarizations were performed to study the electrochemical activity of each alloy after it was exposed to molten nitrate salt at each temperature point using a scan rate of 5 mV/s. A scan rate of 1 mV/s was initially chosen as per previous work in this molten salt system, however, due to the nature of the system and convection currents in the salt during testing, the polarization scans at this scan rate were too noisy to discern meaningful data from and a scan rate of 5 mV/s was chosen.[2] The electrochemical results were then compared to the exposure study and Raman analysis results to evaluate a correlation between the electrochemical results and longer term molten nitrate salt exposure.

Post-exposure analysis of the sample salt was conducted using inductively-couple plasma optical emission spectroscopy (ICP-OES) with a Perkin-Elmer Optima 8000 by dissolving the salt in deionized water containing 72 mM sulfuric acid. Post-exposure analysis of the samples was conducted using X-ray diffraction (XRD) and Raman spectroscopy. XRD patterns were collected using a Rigaku Smartlab 3 kW X-ray diffractometer with a Cu Kα X-ray source ($\lambda = 1.541$ Å; 40 kV and 44 mA) using 2-theta low-incidence angle technique. All patterns were collected over a range of $2\text{-}\theta = 10°–90°$ using a parallel beam with an incidence angle of 1.5 degrees. All diffraction patterns were analyzed using PDXL 2 with the ICDD database. Raman spectra were collected using a Thermo Scientific DXR Raman Microscope equipped with a 10 mW 532-nm laser averaging multiple area map points taken at 500x magnification.

Exposure Study Results

Following exposure to molten nitrate salts, the alloys were observed to have undergone visible degradation. In general, as the temperature of the melt and exposure duration increases, the sample surfaces became more dark as observed in Figure 1. Alloy 4130 maintains a gray to dark gray hue after all exposure conditions, while the greater Cr and Ni content alloys exhibit a golden color after exposure in molten salt at 300°C for 100 hours and becoming a darker gray as time and temperature increased. The sample salt following exposure also exhibited a visual change from a clear liquid prior to exposure to a yellow hue following exposure to SS316 and 800H. Figure 2 shows the salt mixtures to which the alloys were exposed for 100 hours at 500°C. The yellow coloration of the salt is indicative of chromium dissolution as observed previously by Bradshaw[5] and supported by ICP-OES analysis of the salt following exposure as will be discussed later.

Gravimetric analysis results comparing the three alloys across all test conditions are shown in Figure 3. Alloy 4130 experienced a greater weight gain rate compared to SS316 and 800H with a significant increase in weight gain rate from 300°C to 400°C. The weight gain rate of 4130 exposed for 350 hours at 500°C was more than double the rate measured after 100 hours at 500°C. This observation is likely due to the interaction of vapors released from the molten salt mixture with the area of the sample not immersed resulting in the formation of porous oxide layers as observed in previous work with low-Cr content T-22.[15] Additionally, it has been reported in previous work that increased nitrite content of the salt mixture results in enhanced oxidative behavior, and that nitrite is continuously formed as time proceeds due to thermal and electrochemical degradation.[16]

Stainless steel 316 and Incoloy 800H both experienced significantly lower weight gain rates than Alloy 4130 at 400 and 500°C. SS316 and 800H showed similar weight gain rates at all test conditions in their as-received conditions. However, the 800H samples with one polished face exposed to 500°C for 100 hours showed a lower weight gain rate than both SS316 and 800H as-received samples at the same conditions. The lower weight gain rate of the polished 800H samples is likely a result of increased metallic dissolution from the base metal due to the removal of the possible native oxide film. The weight gain rates for SS316 and 800H were observed to be lower after exposure at 500°C for 350 hours than at 500°C for 100 hours. This behavior can be attributed to surface finish effects or time-dependent equilibration that requires more than 100 hours to achieve. This behavior has been observed in other works studying OC-4 steel in molten nitrate salt.[17]

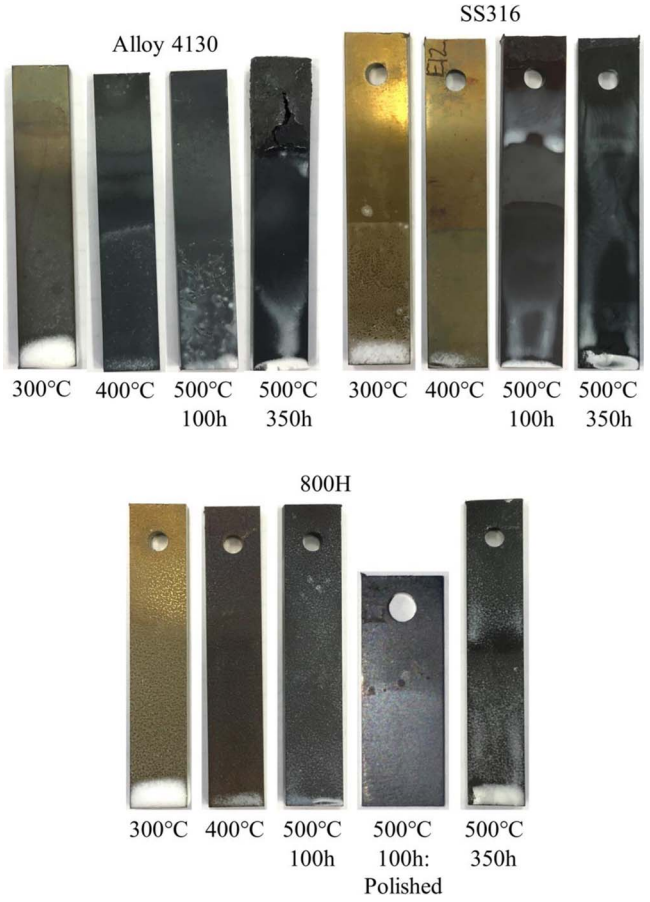

Figure 1. Digital photographs of samples comparing the visual differences after exposure to molten nitrate salt. The images compare the visual darkening of the sample surface after 100 hours as the temperature of the salt increased from 300°C to 500°C. The visual differences between the samples exposed for 100 hours and 350 hours at 500°C are also compared. While no visible change was observed in the exposed area of the 350 hour 4130 sample, the area exposed to the vapor phase of the salt after 350 hours is significantly degraded. Note: Polished 800H sample image enlarged to compare coloration, not to scale with other samples.

Post-exposure salt chemistry analysis.—The dissolution rates of alloying elements as measured by ICP-OES of the sample melts for each alloy and condition is presented in Figure 4. As expected, based on the color expressed by the molten salt after exposure as shown in Figure 2, chromium was the most prominent alloying element found in the molten salt solution followed by nickel and iron. The dissolution of chromium during exposure suggests that the passive film normally associated with corrosion resistant alloys was not present in this environment. The oxidation state of the Cr anion in the melt has been suggested to be hexavalent chromium from previous work in molten nitrate salts.[4] Other studies have suggested that hexavalent Cr begins as dichromate ($Cr_2O_7^{2-}$) and proceeds at a measurable rate to chromate (CrO_4^{2-}) at 250°C in a eutectic $NaNO_3/KNO_3$ mixture which produces the yellow color observed in the melt following exposure.[18]

The dissolution rate of chromium for the different alloys is interesting to note. A more concise comparison is shown in Figure 5. The dissolution of chromium, in general, increased with temperature which supports the claim made by Bradshaw[5] that suggests that the depletion of chromium is diffusion controlled. Diffusion control can also explain why the dissolution rates in as-received SS316 and 800H do not increase after 350 hours compared to 100 hours. Conversely, the dissolution rate observed for the Alloy 4130 samples exposed for 350 hours at 500°C was greater than that observed for 4130 samples exposed for 100 hours at 500°C. The higher rate is most likely a result of the oxide spallation that led to electrolyte infiltration into the oxide scale thus increasing the area of interaction and diffusion rate. Due to the exposure area of the samples used for dissolution rate calculations being measured as the geometric areas that were immersed in the molten salt, the dissolution rate of Cr in the 4130 sample exposed for 350 hours at 500°C is overestimated due to underestimation of the exposed area. The depletion of chromium from the polished 800H samples was found to be comparable to as-received SS316 under the same conditions, and the rate observed for as-received 800H after 350 hours. The marked difference between as-received and polished 800H at 500°C suggests that the surface finish

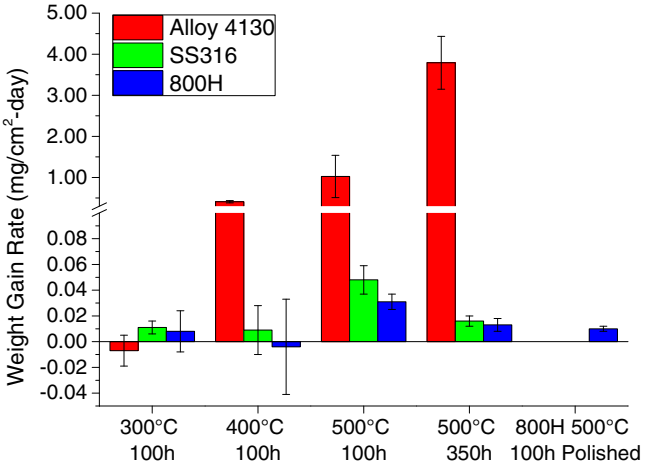

Figure 3. Weight gain rate for alloys 4130, SS316 and 800H showing the greater oxidation rate of Alloy 4130 compared to SS316 and 800H. SS316 and 800H show similar weight gain rates.

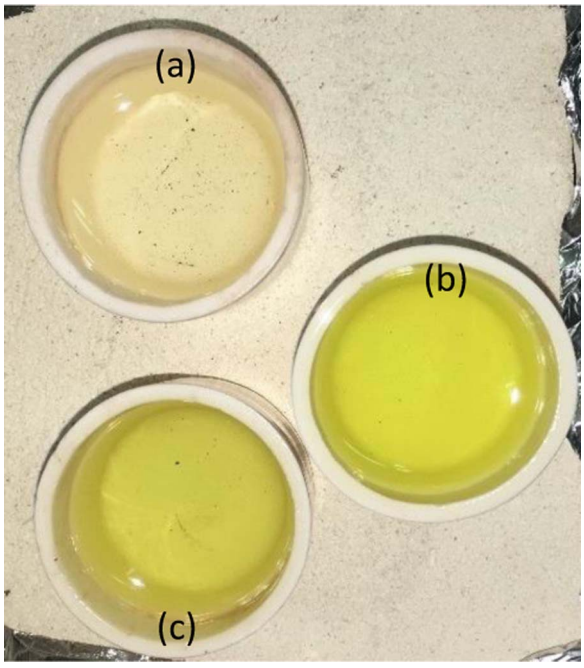

Figure 2. Digital photograph of the molten salt mixtures used to expose (a) Alloy 4130, (b) Incoloy 800H and (c) Stainless Steel 316 for 100 hours at 500°C. The difference in coloration is likely due to chromium leached from each of the samples explaining why the color of the salt in which Alloy 4130 was exposed remained unchanged. This is supported by significant levels of chromium discovered in the melt by ICP-OES analysis.

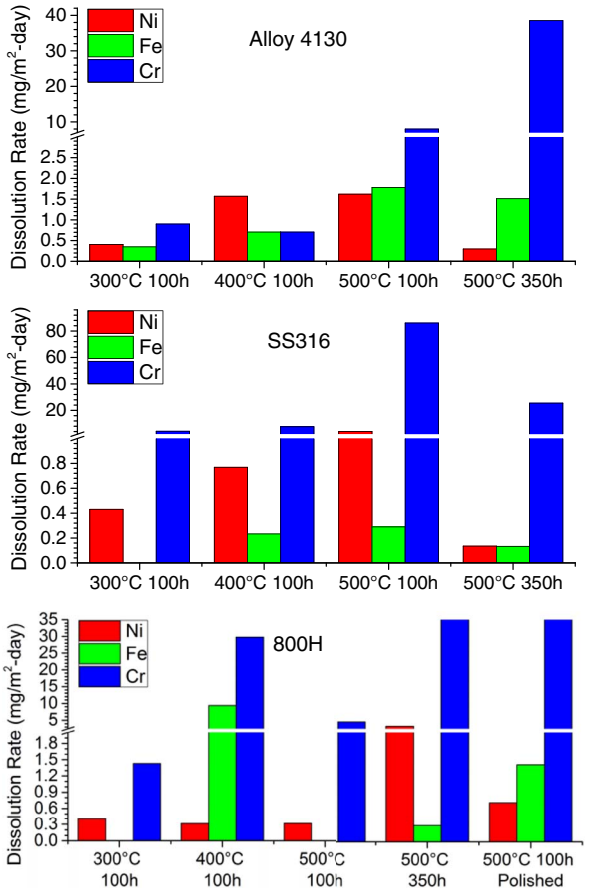

Figure 4. Metallic dissolution rates for Alloy 4130, SS316 and 800H salt melts after exposure. Ni, Fe, and Cr were identified as the prominent dissolved products. This shows that chromium is the most prominent alloying element present in solution.

has a significant influence on the alloy's performance. However, the fact that nearly the same rate as the polished samples was observed for the as-received samples after 350 hours suggests that the as-received surface finish only slows the kinetics of Cr dissolution at short time scales.

SS316 shows a lower dissolution rate of nickel, iron, and chromium after 350 hours than was observed after 100 hours. The lower dissolution rate for these elements also corresponds with a lower weight gain rate which may suggest the formation of a protective oxide layer after 100 hours that decreases the diffusion rate of these elements and thus lowers the dissolution rate and rate of oxide formation.

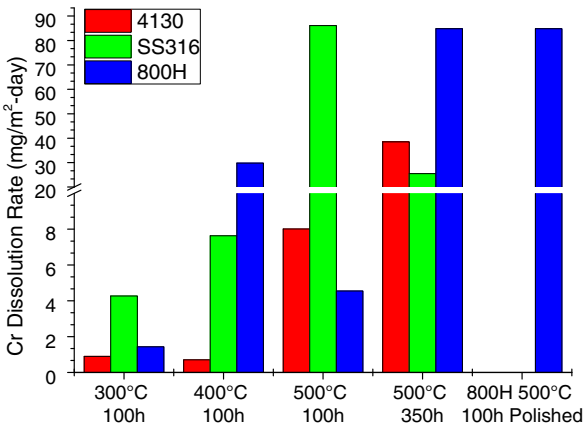

Figure 5. Comparison of chromium dissolution rates for Alloy 4130, SS316 and 800H after 100 hour exposures at 300, 400, 500°C and 500°C for 350 hours. Additionally, the dissolution rate of the polished 800H salt solution is shown. Although much lower in Cr content, Alloy 4130 showed a significant amount of Cr dissolution compared to the higher Cr-content alloys.

Raman spectroscopy.—The Raman spectra obtained from the surface of Alloy 4130 exposed for 100 hours at 300°C, 400°C, 500°C and for 350 hours at 500°C are shown in Figure 6. The primary features observed were magnetite (Fe_3O_4) at ~ 672 cm^{-1}, hematite (α-Fe_2O_3) at ~227, 292, 497 and 1320 cm^{-1}, and maghemite (γ-Fe_2O_3) by broad peaks at 350–352 and ~700 cm^{-1}. The feature associated with magnetite is in good agreement with other studies on Raman spectra of iron oxides.[19–23] Hematite features observed on these samples were also in agreement with numerous studies on iron oxides.[21,24–27] The maghemite features observed on these samples are in agreement with literature with respect to position and shape.[19,24,27] The presence of potassium nitrite (KNO_2) and sodium nitrite ($NaNO_2$) as features in the Raman spectra of the sample surfaces were recorded as the presence of these compounds in molten solar salt have been reported by multiple authors as the result of thermal decomposition and as the primary mechanism for oxidation of species in this melt.[9,28–30] Maghemite (γ-Fe_2O_3) was an unexpected iron oxide to observe as it is an intermediate product in the formation of α-Fe_2O_3 from Fe_3O_4 as temperature increases and is not a stable phase of Fe_2O_3.[24,31–33] The oxidation process of iron in molten nitrate/nitrite salts has been explored through electrochemical methods in past work that suggests that the following partial reactions participate to differing degrees with changes in temperature where the parenthetical species are adsorbed layers on the iron substrate.[13]

$$Fe(Fe_3O_4)(NO_2) \rightarrow Fe(Fe_3O_4) + NO_2 \quad [1]$$

$$Fe(Fe_3O_4)(NO_2) \rightarrow Fe(Fe_2O_3) + NO \quad [2]$$

$$Fe(Fe_3O_4)(NO_2) + NO_2^- \rightarrow Fe(Fe_3O_4) + NO_3^- + NO \quad [3]$$

Additionally, it has been shown in previous works that iron in the presence of nitrate salts passivates to magnetite with traces of FeO. Once passivated, oxidation of nitrite ions (NO_2^-) takes place forming nitrogen dioxide (NO_2) which may contribute to the oxidation of Fe and Fe_3O_4 via the reduction to nitrous oxide (N_2O).[9] Therefore, the presence of maghemite may be explained by the incomplete oxidation of magnetite to hematite in a quantity detectable by Raman spectroscopy. This oxidation mechanism gives insight into the reactions occurring during electrochemical testing and a correlation between surface characterization results and molten salt-alloy interactions.

The Raman spectra of SS316 exposed for 100 hours at 300°C, 400°C, 500°C and for 350 hours at 500°C are shown in Figure 6. The predominant features observed on SS316 samples at 500°C were those corresponding to hematite at ~224, 242, 290, 406, 609 and 1314 cm^{-1} which were in good agreement with literature values.[21,22,24–27] At 300 and 400°C, the predominant features were those that agree well with literature values for nickel ferrite ($NiFe_2O_4$) at ~496, 658 and 706 cm^{-1}.[25,26,34,35] Due to the similarities of magnetite and nickel ferrite Raman features, there is a possibility that the broad peak in the 650–710 cm^{-1} region is a convolution of the two spinels; however, the features indicative of nickel ferrite are in better agreement with the recorded spectra than magnetite and have been labeled as such.

The Raman spectra of Incoloy 800H samples exposed for 100 hours at 300°C, 400°C, 500°C and for 350 hours at 500°C are shown in Figure 6. The Raman features observed on samples exposed at 300 and 400°C are in good agreement with literature values for nickel ferrite at ~339, 499, 576, 663 and 705 cm^{-1}.[25,26,34,35] Similar to SS316, 800H samples exposed to 500°C after 100 and 350 hours expressed Raman features dominated by hematite at ~225, 247, 293, 409, 612 and 1316 cm^{-1}, in agreement with literature, with nickel ferrite bands decreasing in intensity compared to samples exposed to lower temperatures.[20–22,25–27] The Raman spectra of the polished surface of the 800H sample exposed for 100 hours at 500°C

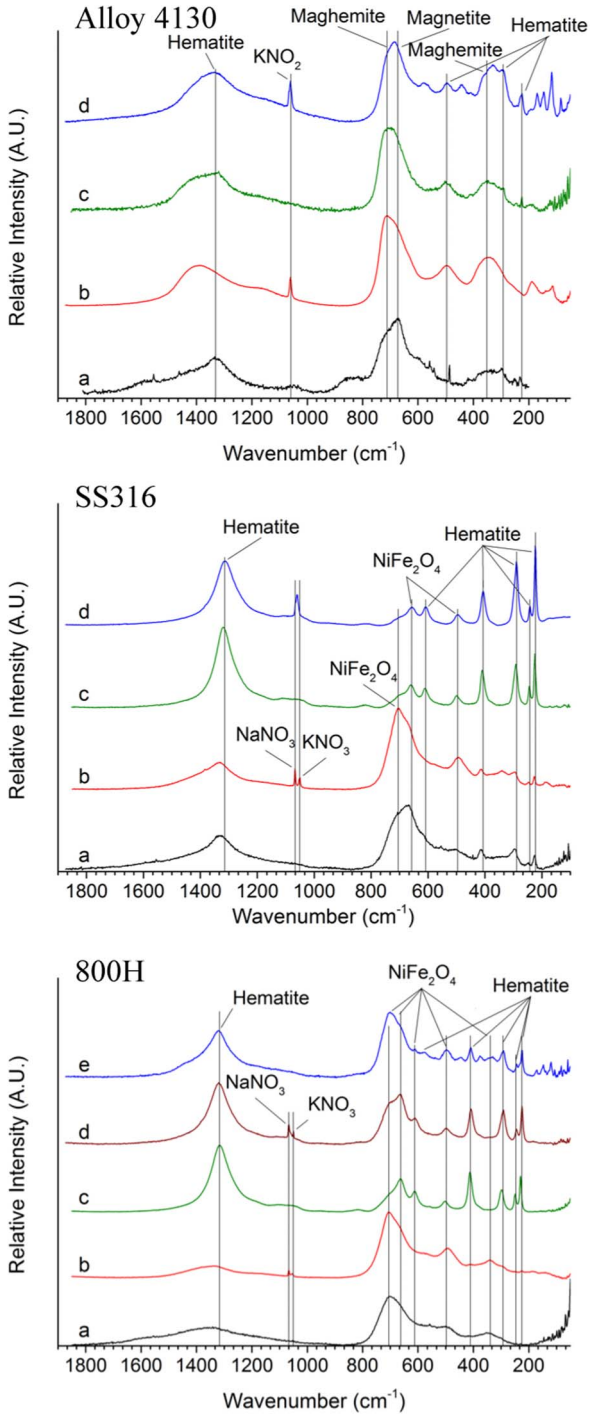

Figure 6. Raman spectra of Alloy 4130, SS316 and 800H samples exposed to molten nitrate salt for 100 hours at (a) 300°C, (b) 400°C, (c) 500°C, (d) 350 hours at 500°C and (e) 500°C polished. Comparison of the spectra shows a shift in the composition of the oxide from a spinel to primarily hematite above 300°C. While as-received 800H exposed for 100 hours at 300°C and 400°C were similar, as-received samples exposed to 500°C molten salt expressed different features with predominantly hematite features. However, the polished sample exposed to 500°C for 100 hours showed a shift to nickel ferrite.

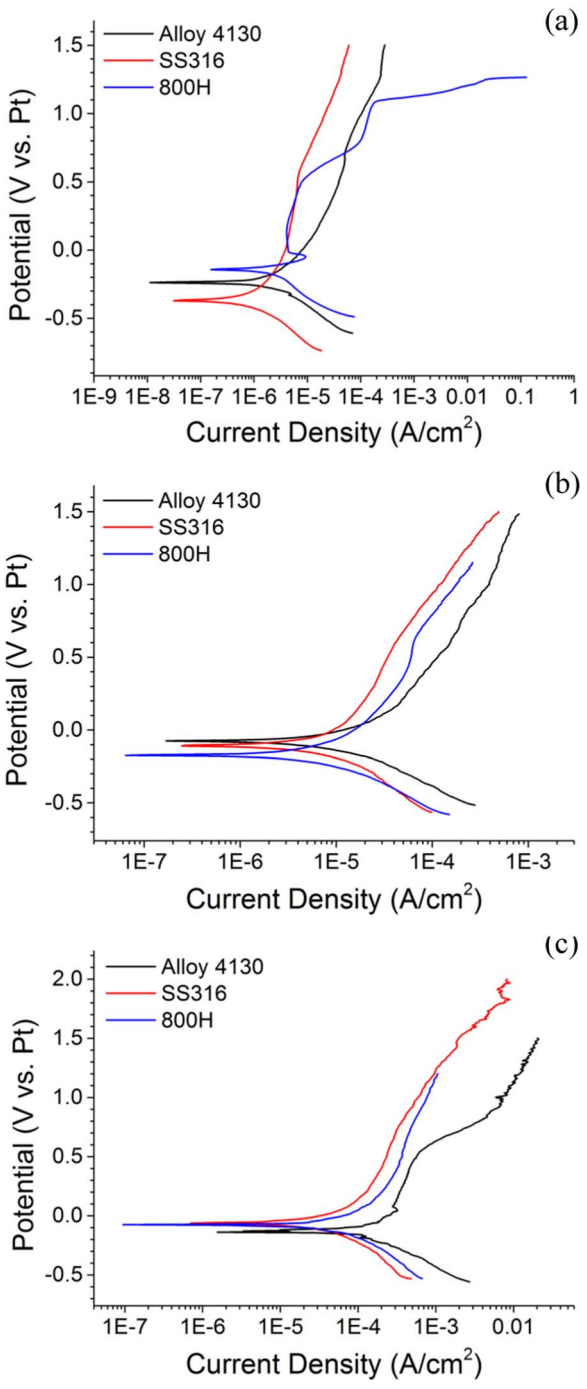

Figure 7. Potentiodynamic polarizations of Alloy 4130, SS316, and 800H at (a) 300°C, (b) 400°C and (c) 500°C. The polarization response of each alloy at each temperature were similar, but the trend between the three alloys shows that Alloy 4130 is the most active alloy and that SS316 and 800H exhibited similar electrochemical response.

compared to the as-received samples exposed for 100 and 350 hours at the same temperature differ in the ratio of hematite to nickel ferrite. The hematite features on the polished samples were suppressed, while the primary nickel ferrite feature at ~705 cm^{-1} increased in intensity. The difference in Raman spectra between polished and as-received samples shows that surface effects have an influence on corrosion characteristics in molten nitrate salts similar to aqueous environments.[36,37]

Electrochemical Evaluation Results

To evaluate how the corrosion resistance of each alloy is affected by temperature, a quasi-reference electrode utilizing a platinum wire was used. Although the platinum wire reference is not thermodynamically constrained, it has been utilized for the determination of electrode interactions with molten nitrate salts in previous work.[14] Figure 7a compares the polarizations of Alloy 4130, SS316, and 800H at 300°C.

800H was the only alloy to indicate that passivation occurs at 300°C. SS316 was the most electrochemically active alloy at this temperature. These electrochemical results correlate well with the gravimetric and ICP-OES analysis. SS316 had the greatest mean weight gain rate and second greatest chromium dissolution rate, while 800H had the lowest chromium dissolution rate.

Figure 7b shows a comparison of polarizations performed in Alloy 4130, SS316, and 800H at 400°C. At this temperature, the polarizations of each alloy are nested closely together. The corrosion potentials fall within a 100 mV range with Alloy 4130 exhibiting a corrosion potential closest to 0 V, and 800H was the most negative. These relative potentials suggest that 800H is the most electrochemically active alloy and 4130 is the least active. This suggestion is at odds with the gravimetric data which shows 4130 with the highest weight gain rate. However, the greatest Cr dissolution rate was observed from 800H at 400°C which correlates well with 800H being the most electrochemically active alloy.

Figure 7c compares the polarizations of Alloy 4130, SS316, and 800H in 500°C molten nitrate salt. Similar to polarizations performed at 400°C, the corrosion potentials of the alloys were all in a 75 mV range which suggests that all three alloys have similar thermodynamic behavior. The polarizations of SS316 and 800H are nearly identical and a corrosion potential difference of only ∼13 mV makes determining which alloy is less active difficult. The current response of Alloy 4130 was greater than SS316 and 800H which correlates with a more kinetically active electrode. The data obtained from electrochemical analysis correlates well with gravimetric and ICP-OES data. It was observed that Alloy 4130 had the greatest weight gain at 500°C. SS316 and 800H displayed similar weight gain and chromium dissolution which agrees with the similar electrochemical response.

Discussion

The correlation between the electrochemical results and the exposure study analysis is difficult to discern due to a combination of interactions that are occurring at the metal-salt interface. Based on the evidence from Raman and ICP-OES analysis, the alloys are being oxidized in the presence of molten nitrate salts which is resulting in the formation of iron oxides on the surface and preferential removal of chromium. This balance of preferential Cr dissolution and iron oxidation makes correlating the electrochemical response of the alloys in this environment more complex. As is shown in Figure 7b and 7c, the corrosion potentials of the three alloys are relatively similar which requires one to also look at the current response of the polarization. While the corrosion potentials indicate the thermodynamic potential for reaction, the current response measures the kinetics of the reactions taking place which include the formation of relatively adherent iron oxides and dissolution of Cr in the form of chromates and dichromates. Therefore, the corrosion potential should become more negative versus a platinum reference if the alloy is more electrochemically active. Additionally, the current response should be greater for alloys that are more electrochemically active. Depending on the environment that the alloy is in, the alloy may be more thermodynamically or kinetically active and thus the electrochemical correlation with exposure study results may be a comparison of the corrosion potentials or of the current responses. However, the aim of this study is to test the feasibility of using electrochemical polarization to compare corrosion behavior of potential alloys in molten nitrate salts. This study also used a pseudo-reference for electrochemical experiments. Therefore, the results of this study suggest that electrochemical polarization may be used for such a purpose, but further studies should be performed using a more stable reference electrode to verify these findings.

The gravimetric, ICP-OES, and Raman data helped to better correlate the electrochemical results and understand what metal-salt interactions may be affecting those results. Based on the results from the exposure study analysis, reactions 1–3 discussed earlier appear to be the primary oxidation mechanism occurring due to exposure to molten nitrate salt. The ICP-OES results of the salt, post-exposure, show that Cr was being preferentially brought into solution from all

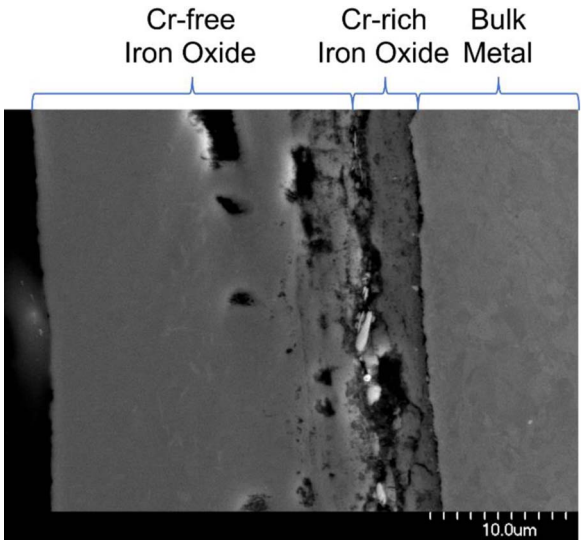

Figure 8. Scanning electron micrograph of Alloy 4130 exposed to molten nitrate salt for 100 hours at 500°C cross-sectioned to show the layered structure of the oxide film. Energy-dispersive spectroscopic analysis indicated that the dense, outer oxide layer is composed of iron oxide, while Cr was detected in the inner, porous oxide at the metal-oxide interface.

alloy compositions. The cross-sectional SEM-EDS analysis of 4130 shown in Figure 8 also indicates that Cr is depleted from the outer oxide layer and a denser iron oxide layer is formed. The oxide layer is not protective, however, due to the inner, porous oxide layer which is likely formed due to cation vacancy migration from the oxide-salt interface to the metal-oxide interface common in high temperature corrosion.[38] The migration of cation vacancies inward would also suggest lattice cation migration outwards to the oxide-salt interface which may explain the apparent leaching of Cr and densification of the outer oxide layer. Other works that perform longer term exposure studies on similar alloys also show Cr dissolution and the formation of a non-protective iron oxide surface film.[7,8,39]

Summary

Low alloy steel (Alloy 4130) performed well in molten nitrate salt maintained at 300°C showing little to no weight gain or corrosion after 100 hours. Based on electrochemical analysis, Alloy 4130 is expected to perform as well as SS316 or 800H which is supported by gravimetric measurements and ICP-OES results. Despite the low-Cr content of Alloy 4130, significant dissolution of Cr was observed at all temperatures investigated, although it was lower than dissolution from other two alloys which contained greater amounts of chromium. Results from XRD and Raman spectroscopy indicated that magnetite was the dominant oxide formed at lower temperatures, while hematite was the dominant oxide formed at higher temperatures.

SS316 and Incoloy 800H both performed well at all temperatures showing acceptable weight gain. ICP-OES analysis indicated significant chromium dissolution from both alloys, the rate of which increased with temperature. An anomalous chromium dissolution rate observed for 800H after 100 hours of exposure in molten salt maintained at 500°C prompted the exploration of surface finish by polishing three samples and exposing them for 100 hours at 500°C. The chromium dissolution of these samples was then found to be in agreement with the trend of increasing rate with increasing temperature and matched that of the as-received 800H samples exposed for 350 hours at 500°C.

Electrochemical evaluation of Alloy 4130, SS316, and 800H were performed at 300, 400, and 500°C versus a platinum reference electrode. Comparison of potentiodynamic polarization scans at each temperature indicated behavior resembling the trends observed following

analysis of exposure study results. These results suggest that electrochemical evaluation of corrosion behavior may potentially be utilized as a means of screening candidate materials for use in molten nitrate salts. However, further long term exposure studies and accelerated electrochemical studies using a standard reference electrode are suggested.

Acknowledgments

This work funded in part by the National Science Foundation under grant No. IIA-1301726.

References

1. W. R. Delameter and N. E. Bergan, *Review of the Molten Salt Electric Experiment: A solar central receiver project*, in, p. Medium: ED; Size: Pages: 34, Sandia National Labs., Livermore, CA (USA) (1986).
2. I. B. Singh, *Corrosion science*, **37**, 1981 (1995).
3. R. Dölling, H. Holtan, A. Sterten, and R. Tunold, *Materials and Corrosion/Werkstoffe und Korrosion*, **31**, 470 (1980).
4. P. F. Tortorelli and J. H. DeVan, *Thermal-convection-loop study of the corrosion of Fe-Ni-Cr alloys by molten $NaNO_3$-KNO_3*, in, Oak Ridge National Lab., TN (USA) (1982).
5. R. W. Bradshaw, *Corrosion*, **43**, 173 (1987).
6. R. W. Bradshaw and R. W. Carling, *A review of the chemical and physical properties of molten alkali nitrate salts and their effect on materials used for solar central receivers*, in, Sandia National Labs., Livermore, CA (USA) (1987).
7. R. W. Bradshaw and S. H. Goods, *Corrosion resistance of stainless steels during thermal cycling in alkali nitrate molten salts*, in, Sandia Nat. Lab. (2001).
8. S. H. Goods and R. W. Bradshaw, *Journal of Materials Engineering and Performance*, **13**, 78 (2004).
9. A. J. Arvía, J. J. Podestá, and R. C. V. Piatti, *Electrochimica Acta*, **17**, 33 (1972).
10. R. W. Bradshaw and D. E. Meeker, *Sol Energ Mater*, **21**, 51 (1990).
11. R. W. Mar and C. M. Kramer, *Sol Energ Mater*, **5**, 71 (1981).
12. B. Bond and P. Jacobs, *Journal of the Chemical Society A: Inorganic, Physical, Theoretical*, 1265 (1966).
13. A. J. Arvía, J. J. Podestá, and R. C. V. Piatti, *Electrochimica Acta*, **16**, 1797 (1971).
14. S. L. Marchiano and A. J. Arvía, *Electrochimica Acta*, **17**, 25 (1972).
15. A. Fernandez, M. Lasanta, and F. Perez, *Oxidation of metals*, **78**, 329 (2012).
16. H. Swofford Jr and P. McCormick, *Analytical Chemistry*, **37**, 970 (1965).
17. A. Fernández, A. Rey, I. Lasanta, S. Mato, M. Brady, and F. Pérez, *Materials and Corrosion*, **65**, 267 (2014).
18. F. R. Duke and M. L. Iverson, *Journal of the American Chemical Society*, **80**, 5061 (1958).
19. N. Boucherit, A. Hugot-Le Goff, and S. Joiret, *Corrosion Science*, **32**, 497 (1991).
20. J. Dünnwald and A. Otto, *Corrosion Science*, **29**, 1167 (1989).
21. K. F. McCarty and D. R. Boehme, *Journal of solid state chemistry*, **79**, 19 (1989).
22. D. Rodriguez, A. Merwin, and D. Chidambaram, *Journal of Nuclear Materials*, **452**, 440 (2014).
23. D. Thierry, D. Persson, C. Leygraf, N. Boucherit, and A. Hugot-Le Goff, *Corrosion Science*, **32**, 273 (1991).
24. D. L. A. De Faria, S. Venâncio Silva, and M. T. De Oliveira, *Journal of Raman spectroscopy*, **28**, 873 (1997).
25. B. D. Hosterman, *Raman spectroscopic study of solid solution spinel oxides, in Physics and Astronomy*, p. 155, University of Nevada, Las Vegas (2011).
26. Z. Karmiol, *Comparison of Nitronic 50 and Stainless Steel 316 for use in Supercritical Water Environments*, (2014).
27. T. Ohtsuka, K. Kubo, and N. Sato, *Corrosion*, **42**, 476 (1986).
28. R. N. Kust and J. D. Burke, *Inorganic and Nuclear Chemistry Letters*, **6**, 333 (1970).
29. D. Nissen and D. Meeker, *Inorganic Chemistry*, **22**, 716 (1983).
30. I. B. Singh, S. Sultan, and K. Balakrishnan, *Electrochimica acta*, **40**, 1755 (1995).
31. P. S. Sidhu, *Clay Clay Miner*, **36**, 31 (1988).
32. F. E. DeBoer and P. W. Selwood, *Journal of the American Chemical Society*, **76**, 3365 (1954).
33. G. Yasumasa, *Japanese Journal of Applied Physics*, **3**, 739 (1964).
34. P. R. Graves, C. Johnston, and J. J. Campaniello, *Materials Research Bulletin*, **23**, 1651 (1988).
35. J. H. Kim and I. S. Hwang, *Nuclear Engineering and Design*, **235**, 1029 (2005).
36. W. E. Ruther, R. R. Schlueter, R. H. Lee, and R. K. Hart, *Corrosion*, **22**, 147 (1966).
37. M. Warzee, J. Hennaut, M. Maurice, C. Sonnen, J. Waty, and P. Berge, *Journal of the electrochemical society*, **112**, 670 (1965).
38. D. A. Jones, *Principles and prevention of corrosion*, Macmillan (1992).
39. A. Fernández, H. Galleguillos, E. Fuentealba, and F. Pérez, *Solar Energy Materials and Solar Cells*, **141**, 7 (2015).